Funneling Light through a Subwavelength Aperture with Epsilon-Near-Zero Materials

D. C. Adams,[1] S. Inampudi,[1] T. Ribaudo,[1] D. Slocum,[1] S. Vangala,[1] N. A. Kuhta,[2] W. D. Goodhue,[1] V. A. Podolskiy,[1] and D. Wasserman[1]

[1]*University of Massachusetts Lowell, Lowell, Massachusetts 01854, USA*

[2]*Oregon State University, Corvallis, Oregon 97331, USA*

(Received 14 April 2011; published 19 September 2011)

We present a comprehensive study of enhanced light funneling through a subwavelength aperture with realistic (lossy) epsilon-near-zero (ENZ) materials. We realize experimentally an inclusion-free ENZ material layer operating at optical frequencies and characterize its performance. An analytical expression describing light funneling through several structures involving ENZ coupling layers is developed, validated with numerical solutions of Maxwell equations, and utilized to relate the performance of the ENZ coupling systems to their main limiting factor, material losses.

DOI: 10.1103/PhysRevLett.107.133901 PACS numbers: 42.79.Gn, 42.70.Km, 78.66.Fd, 78.67.Pt

Integration of the next generation of photonic structures with electronic and optical on-chip components requires the development of effective methods for confining and controlling light in subwavelength volumes. Several techniques enabling light coupling to subwavelength objects have recently been proposed, including grating- [1–3], and composite-based solutions [4–8]. However, experimental realization of such structures involves complex, high-resolution ($\sim$ 10 nm) fabrication. One promising alternative to such structures relies on materials with vanishingly small dielectric permittivity, also known as epsilon-near-zero (ENZ) materials [9,10]. In contrast to the previously referenced approaches, a single flat layer of ENZ material is expected to provide efficient coupling between free-space radiation and subwavelength guiding systems.

ENZ materials are known to possess some unusual properties [9]. In particular, the electromagnetic field inside the ENZ structures tends to become completely homogeneous, reflecting the dramatic extension of local wavelength caused by a vanishingly small refractive index. It has been shown theoretically [10,11] that lossless ENZ systems may yield perfect coupling between two planar waveguides through an ultrathin guiding channel. Experimental verifications of this principle, in the microwave regime, utilized split ring resonator structures [12] or, alternatively, waveguides designed to mimic the optical properties of an ENZ material [11,13]. An alternative mechanism for ENZ-enhanced transmission of plane waves through a relatively thick ENZ cover, discussed by using a ray optics "focusing" formalism, was presented in Ref. [14]. However, to the best of our knowledge, up to now the majority of theoretical studies of ENZ-enhanced transmission either neglected material absorption or considered unrealistically low losses, and no experiments with homogenous ENZ materials have been performed.

In this work, we first present the first experimental study of ENZ-enhanced transmission through subwavelength features with a homogenous ENZ material. Our material is semiconductor-based and inclusion-free and operates at optical frequencies (in the midinfrared wavelength range). We then present an analytical description of this unique phenomenon. Finally, we propose the optimal geometry for ENZ-enhanced transmission with realistic (lossy) materials. Our study opens the door to multiple practical applications of ENZ materials and ENZ-based photonic systems.

The ENZ material used in this experiment consists of the heavily doped, narrow band-gap semiconductor $InAs_xSb_{1-x}$, with $x = 0.89$. Our InAsSb layer was grown by molecular beam epitaxy in a Riber 32 system, on a semi-insulating GaAs substrate. The InAsSb epilayer is 1.15 μm thick and heavily n-doped (~ 1–2×10^{19} cm^{-3}). The conduction band electrons in semiconductors behave as a free-electron plasma, whose interaction with incident radiation can be described by a Drude-like dispersion. Therefore, the permittivity of the semiconductor can be represented as

$$\epsilon(\omega) = \epsilon_\infty\left(1 - \frac{\omega_p^2}{\omega^2 + i\omega\Gamma}\right), \qquad \omega_p^2 = \frac{ne^2}{m^*\epsilon_o\epsilon_\infty}, \quad (1)$$

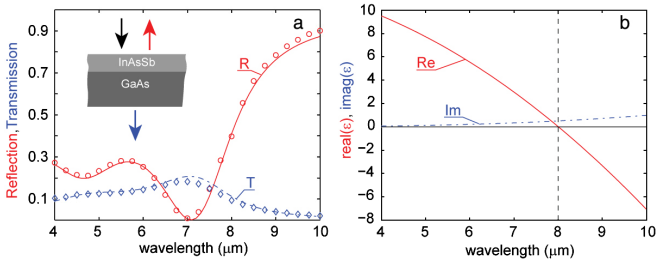

FIG. 1 (color online). (a) Schematic of the as-grown ENZ-material optical measurements (inset) and the transmission and reflection data from these measurements; symbols show experimental reflection (red circles) and transmission (blue diamonds); lines represent theoretical fits. (b) Retrieved permittivity spectra from the data in (a).

where ω is the radial frequency of the radiation, Γ is the damping constant, ϵ_∞ is the high-frequency permittivity of the semiconductor lattice, ω_p is the semiconductor plasma frequency, n is the carrier concentration, and m^* is the effective mass of the free electrons in the semiconductor [15]. The combination of high doping and low electron mass, realized in the InAsSb material system (and in previous work with InGaAs [16]), pushes ω_p of the material well into the 6–10 μm wavelength range.

The optical properties of our as-grown ENZ layer can be determined from transmission and reflection data collected on the as-grown InAsSb/GaAs wafer, by using the fitting process outlined in Ref. [17], yielding a plasma wavelength ~ 8 μm (~ 1250 cm^{-1}) and the damping constant $\Gamma = 50$ cm^{-1}. To accurately describe absorption due to lattice-mismatch-induced defects in the transition layer between the GaAs substrate and the ENZ layer, we scaled the theoretical transmission data in Fig. 3 by a loss factor $\exp(-2\pi l_0/\lambda)$, with $l_0 \simeq 1.1$ μm. Alternative models of permittivity that do not involve losses in this transitional layer yield qualitatively incorrect results [18].

The resultant spectral dependence of the real (ϵ') and imaginary (ϵ'') parts of the InAsSb permittivity are shown in Fig. 1(b). Note that material losses at the ENZ frequency, represented by the imaginary part of the permittivity, are of the same order as those of noble metals (Ag, Au, etc.) and of transparent conducting oxides, such as indium-tin oxide [19], about their respective ENZ frequencies. Therefore, *our studies provide an outlook for the performance of realistic plasmonic materials across the optical frequency range.*

In order to experimentally demonstrate ENZ-enhanced transmission through subwavelength optical features, subwavelength slits in an optically thick metal layer were fabricated onto the InAsSb epilayer, as shown in Fig. 2, by using standard photolithographic techniques. At the same time, a set of control samples were patterned on a semi-insulating GaAs substrate, in order to compare the ENZ-enhanced transmission to structures with identical geometries, but with minimal material losses. The GaAs substrate, having a relatively large refractive index ($n \simeq 3.3$), represents the best-case scenario for traditional direct coupling of light into the small slit.

The transmission spectra of the ENZ-based and the control structures are shown in Figs. 3(a)–3(c). Slit transmission data were collected on a Bruker IR1 infrared microscope and V70 Fourier transform infrared spectrometer operating in amplitude modulation step-scan mode. The internal spectrometer's globar acts as the incident radiation source, and a wire-grid polarizer, placed in the incident beam path, directly before the sample, allows us to alternate between TM- (electric field perpendicular to the slit) and TE- (electric field parallel to the slit) polarized incident light. The incident radiation is modulated by a beam chopper, and the transmitted radiation is collected by a liquid nitrogen cooled HgCdTe detector coupled to a lock-in amplifier tracking the beam chopper frequency. Data are collected for a spectral range from 700 to 4000 cm^{-1} with 32 cm^{-1} resolution and normalized to transmission through an unpatterned GaAs substrate to remove the

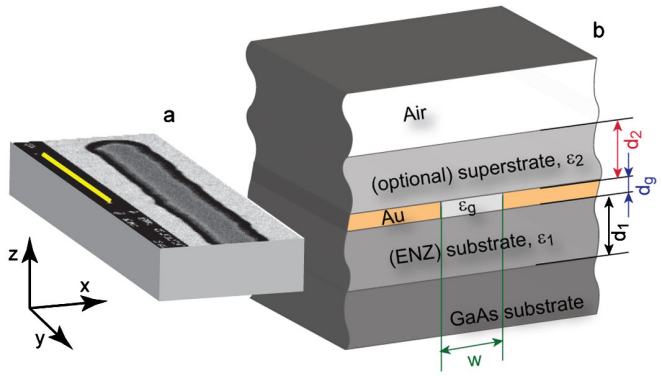

FIG. 2 (color online). (a) Scanning electron microscope image of a representative ENZ-coupled subwavelength aperture used in experiments (length of the yellow scale bar is 6 μm). (b) Schematic drawing of the structure geometry. The total thickness of the ENZ material, n-doped InAsSb, is $d_1 + d_g \simeq 1.15$ μm. The thickness of both the gold and slit is $d_g \simeq 300$ nm. Slit widths (w), between 0.9 and 1.8 μm, were investigated experimentally.

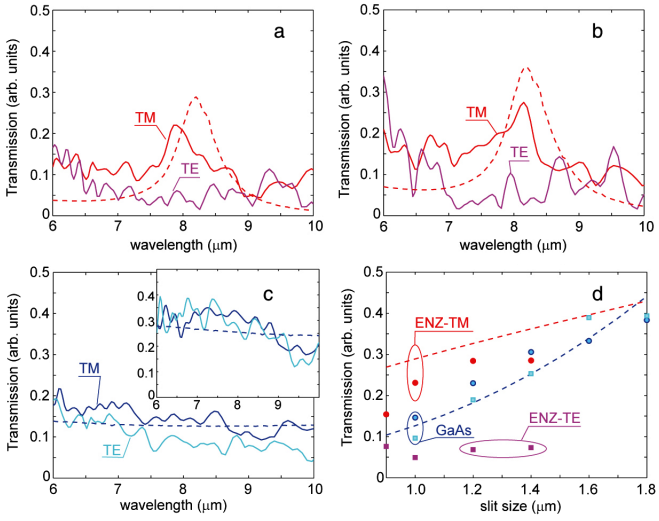

FIG. 3 (color online). Transmission for TM- (red curve) and TE- (magenta curve) polarized light, for systems with (a) $w = 1$ μm and (b) $w = 1.4$ μm. (c) Transmission through the GaAs control structure with $w = 1$ μm (main figure) and $w = 1.4$ μm (inset). (d) Transmission at the ENZ-enhanced transmission peak as a function of slit width w. In all panels, symbols and solid lines correspond to experimental data and dashed lines to analytical results. Analytical results accurately predict off-resonant behavior of relatively small slits ($\sqrt{\epsilon_g} w/\lambda \lesssim 0.5$) while slightly overestimating on-resonant transmission [18]. For thicker slits, higher-mode transmission becomes important.

effects of substrate absorption and spectral features associated with the spectrometer's internal source, the HgCdTe detector, and the focusing and collection optics. Figure 3 shows the TE- and TM-polarized transmission for 1 and 1.4 μm slits fabricated on both the InAsSb and GaAs material. It can clearly be seen that the InAsSb samples provide a drastic enhancement for TM-polarized light coupling into the slit structure at or near the ENZ wavelength. In fact, for each of the ENZ samples tested (0.9, 1.0, 1.2, and 1.4 μm slit sizes), a higher transmission intensity is predicted (and experimentally observed) than for their high-permittivity control counterparts (at $\lambda_0 \sim 8$ μm), despite the significant losses associated with free carriers in the ENZ samples.

To understand the origin of the observed phenomenon, transmission through the system has been modeled with finite-element [20] and with mode-matching software, developed according to Ref. [21], followed by the development of an analytical technique describing transmission and reflection by the system. In this approach, the system under investigation is separated into a set of homogenous layers and a waveguide layer. The field inside the layers is represented as a linear combination of plane waves (free-space modes), parameterized by the x component of their wave vector. The field inside the slit (waveguide) region is represented as a sum of guided (waveguide) modes with their field concentrated inside the slit, accompanied by a set of free-space-like bulk modes with the field extending throughout the metallic cladding. Boundary conditions are used to deduce the arithmetic relationship between the amplitudes of the modes in the adjacent layers. The comparison between the analytical (see below) and numerical solutions of Maxwell equations is presented in Supplemental Materials [18].

To calculate transmission through a subwavelength slit analytically, we represent the incident field as a plane wave with a fixed wave vector k_x^0 ($k_x^0 = 0$ is used in the calculations), and a given amplitude I_0, and approximate the reflected field as a combination of the plane wave with the same wave vector and amplitude R_0 and a scattered wave with the electric field represented as $E_x = S\int e^{i\vec{k}\cdot\vec{r}}\mathrm{sinc}(wk_x/2)dk_x$; the transmitted field is approximated as $E_x = T\int e^{i\vec{k}\cdot\vec{r}}\mathrm{sinc}(wk_x/2)dk_x$ (the spectral shape of the scattered and transmitted fields, representing the field diffracted by a single slit, is consistent with our numerical calculations). Finally, we use the continuity of E_x and H_y along the slit entrance and impedance boundary conditions [22] along the metal surface to deduce the values of the parameters R_0, S, and T and the amplitudes of the fundamental guided mode $A_g^{\pm}$ inside the slit in terms of the parameter I_0.

The overlap-integral formalism, outlined in Refs. [21,23,24], yields the following set of coupled relationships between the parameters:

$$
\begin{aligned}
&I_0 + R_0 + S\frac{2\pi}{w} = A_g^+ + A_g^-\Phi_g,\\
&\frac{\epsilon_1}{k_1^0}[I_0 - R_0 - SI_h(w,\epsilon_1)] = \frac{\epsilon_g}{k_g^0}[A_g^+ - A_g^-\Phi_g],\\
&R_0 = I_0\rho + SI_s(w,\epsilon_1,\epsilon_m,q), \qquad \frac{2\pi}{w}T = A_g^+\Phi_g + A_g^-,\\
&\frac{\epsilon_2}{k_2^0}TI_h(w,\epsilon_2) = \frac{\epsilon_g}{k_g^0}[A_g^+\Phi_g - A_g^-],
\end{aligned}
\tag{2}
$$

where ϵ_1, ϵ_g, ϵ_m, and ϵ_2 describe permittivities of materials in front, inside, around, and behind the slit (Fig. 2), respectively, $k_\alpha(k_x) = \sqrt{\epsilon_\alpha\omega^2/c^2 - k_x^2}$, $k_\alpha^0 = k_\alpha(k_x^0)$, $\Phi_g = \exp(ik_g^0 d_g)$, Fresnel coefficient $\rho = \frac{\epsilon_1 k_m^0 - \epsilon_m k_1^0}{\epsilon_1 k_m^0 + \epsilon_m k_1^0}$, and the integral relationships are given by

$$
I_h(w,\epsilon_\alpha) = k_\alpha^0\int_{-\infty}^{\infty}\frac{\mathrm{sinc}^2(k_x w/2)}{k_\alpha(k_x)}dk_x, \tag{3}
$$

$$
I_s(w,\epsilon_\alpha,\epsilon_\beta,q) = \frac{k_\alpha k_\beta q}{\epsilon_\alpha k_\beta^0 + \epsilon_\beta k_\alpha^0}\int_{-\infty}^{\infty}\frac{\epsilon_\alpha k_\beta(k_x) + \epsilon_\beta k_\alpha(k_x)}{k_\alpha(k_x)k_\beta(k_x)}\frac{k_x\sin(k_x w/2) - q\cos(k_x w/2)}{k_x^2 + q^2}\,\mathrm{sinc}\left(\frac{k_x w}{2}\right)dk_x. \tag{4}
$$

The parameter $q \ll 1$ plays the role of the fitting parameter, fine-tuning the role of the impedance boundary conditions. Our studies indicate that the numerical values of the results only weakly depend on the value of q (see Supplemental Materials [18]). Here we use $q = 0.1$. To account for the effects of the other interfaces (GaAs-ENZ and superstrate-air) either above or below the subwavelength slit, Eqs. (2) are incorporated into a conventional plane-wave transfer-matrix formalism [22].

According to the developed formalism, transmission through the system is dominated by the fundamental ($k_x = 0$) mode of the planar slit waveguide, which exists only for TM light. The amplitude of the fundamental mode, and, correspondingly, the total light transfer through the system, is related to the interplay between two processes: (i) coupling between the incident radiation and the $k_x = 0$ mode at the entrance slit of the device and (ii) propagation of the mode through the slit. The flat ENZ layer at the entrance side of the device drastically enhances the coupling between free space and the slit (guide). This enhancement is related to amplification of the amplitude of the electromagnetic field inside the ENZ material [25]. In our system, this enhancement originates from the bulk plasma resonance of the doped semiconductor.

The secondary enhancement comes about from modal intercoupling between the ENZ-filled guide and the ENZ

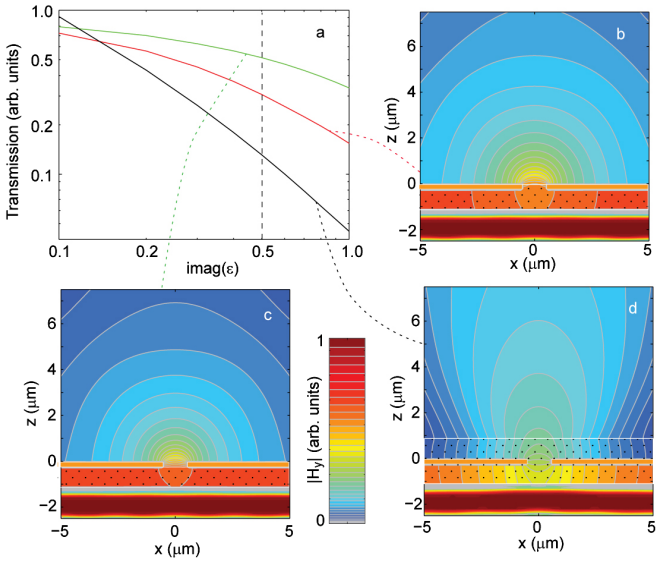

FIG. 4 (color online). (a) Comparison between transmitted power at the ENZ wavelength in three ENZ-assisted structures: (i) the system realized in our experiments (red), when ENZ material fills the substrate and in-slit regions, (ii) the system where the ENZ material is deposited as a thin substrate layer, but air fills both the slit region and the region above the slit (green), and finally, (iii) the design originally suggested in Ref. [14] where ENZ fills substrate, slit, and superstrate regions of the geometry shown in Fig. 2 (black). (b)–(d) illustrate field distribution in the three systems [(i)–(iii), respectively] for $\mathrm{imag}(\epsilon) = 0.1$. The dashed line in (a) represents material loss realized in our experiments.

coupling layer. However, the extra in-coupling efficiency, provided by the ENZ layer inside the waveguide, is more than compensated for by the negative effect of the ENZ-related loss of the device as the mode propagates through the system, which ultimately reduces the amplitude of the fundamental mode at the exit side of the slit. Since the fabrication of ENZ-filled systems is significantly more complicated than the relatively straightforward fabrication of subwavelength geometries above planar ENZ materials, the benefits of complex systems have to be weighed against their expected performance. Such a comparison is shown in Fig. 4. It is seen that, for realistic values of loss, transmission through the subwavelength channel is maximized for structures where the only ENZ component is the thin coupling layer [Fig. 4(b)], and the slit is free of ENZ material. When losses are substantially reduced, however, the positive in-coupling boost provided by the ENZ material inside the slit, accompanied by an ENZ out-coupling layer, adds performance to the system [Fig. 4(d)].

In conclusion, we have reported the comprehensive study of ENZ-enhanced light transmission through an isolated subwavelength slit. An analytical model describing the transmission has been developed, and the interplay between different contributions to ENZ enhancement have been analyzed. Theoretical results are in agreement with experimental data. The work opens the door for ENZ-enhanced coupling to a variety of subwavelength plasmonic, beam-steering, nanophotonic, and nanoelectronic [4,6,7,26–31] systems across a broad frequency range.

The authors gratefully acknowledge N. Engheta (UPenn) for useful discussion and comments. The scanning electron microscopy image in Fig. 2 was taken by D. Safford at IES Technical Sales with a PhenomWorld scanning electron microscope model PHENOM. This work was supported by the AFOSR Young Investigator Program under Grant No. FA9550-10-1-0226 and NSF Grant No. ECCS-0724763.

[1] R. Merlin, Science **317**, 927 (2007).
[2] L. Markley, A. Wong, Y. Wang, and G. Eleftheriades, Phys. Rev. Lett. **101**, 113901 (2008).
[3] S. Thongrattanasiri and V. Podolskiy, Opt. Lett. **34**, 890 (2009).
[4] J. Pendry, Phys. Rev. Lett. **85**, 3966 (2000).
[5] Z. Liu, H. Lee, Y. Xiong, C. Sun, and X. Zhang, Science **315**, 1686 (2007).
[6] Z. Jacob, L. Alekseyev, and E. Narimanov, Opt. Express **14**, 8247 (2006).
[7] A. Salandrino and N. Engheta, Phys. Rev. B **74**, 075103 (2006).
[8] I. Smolyaninov, Y. Hung, and C. Davis, Science **315**, 1699 (2007).
[9] R. Ziolkowski, Phys. Rev. E **70**, 046608 (2004).
[10] M. Silveirinha and N. Engheta, Phys. Rev. Lett. **97**, 157403 (2006).
[11] K. Halterman and S. Feng, Phys. Rev. A **78**, 021805 (2008).
[12] R. Liu, Q. Cheng, T. Hand, J. Mock, T. Cui, S. Cummer, and D. Smith, Phys. Rev. Lett. **100**, 023903 (2008).
[13] B. Edwards, A. Alu, M. Young, M. Silveirinha, and N. Engheta, Phys. Rev. Lett. **100**, 033903 (2008).
[14] A. Alu, F. Bilotti, N. Engheta, and L. Vegni, IEEE Trans. Antennas Propag. **54**, 1632 (2006).
[15] E. Lifshitz and L. Pitaevskii, *Physical Kinetics*, Landau and Lifshitz Course of Theoretical Physics Vol. 10 (Reed, Oxford, 1984).
[16] A. Hoffman, L. Alekseyev, S. Howard, K. Franz, D. Wasserman, V. Podolskiy, E. Narimanov, D. Sivco, and C. Gmachl, Nature Mater. **6**, 946 (2007).
[17] Y. B. Li, R. A. Stradling, T. Knight, J. R. Birch, R. H. Thomas, C. C. Phillips, and I. T. Ferguson, Semicond. Sci. Technol. **8**, 101 (1993).
[18] See Supplemental Material at http://link.aps.org/supplemental/10.1103/PhysRevLett.107.133901 for discussion of alternative models for permittivity, scaling of analytical data, and accuracy of numerical simulations.
[19] A. Boltasseva and H. Atwater, Science **331**, 290 (2011).
[20] http://www.comsol.com.
[21] S. Thongrattanasiri, J. Elser, and V. Podolskiy, J. Opt. Soc. Am. B **26**, B102 (2009).

[22] M. Born and E. Wolf, *Principles of Optics* (Cambridge University Press, Cambridge, England, 1999).
[23] V. V. Schevchenko, *Continuous Transitions in Open Waveguides* (Golem, Boulder, CO, 1971).
[24] J. Bravo-Abad, L. Martin-Moreno, and F. Garcia-Vidal, Phys. Rev. E **69**, 026601 (2004).
[25] Y. Jin, P. Zhang, and S. He, Phys. Rev. B **82**, 075118 (2010).
[26] T. W. Ebbesen, H. J. Lezec, H. F. Ghaemi, T. Thio, and P. A. Wolff, Nature (London) **391**, 667 (1998).
[27] H. Lezec, A. Degiron, E. Devaux, R. Linke, L. Martin-Moreno, F. Garcia-Vidal, and T. Ebbesen, Science **297**, 820 (2002).
[28] J. Pendry, D. Schurig, and D. Smith, Science **312**, 1780 (2006).
[29] W. Cai, U. Chettiar, A. Kildishev, and V. Shalaev, Nat. Photon. **1**, 224 (2007).
[30] A. Kildishev and V. Shalaev, Opt. Lett. **33**, 43 (2008).
[31] N. Engheta, Science **317**, 1698 (2007).